*Article*

# Photooxidation of 2,2′-(Ethyne-1,2-diyl)dianilines: An Enhanced Photocatalytic Properties of New Salophen-Based Zn(II) Complexes

**Mahesh Subburu [1], Ramesh Gade [1], Prabhakar Chetti [2],\* and Someshwar Pola [1],\***

[1] Department of Chemistry, Osmania University, Hyderabad 500007, India; maheshsubburu@gmail.com (M.S.); rameshgade.chem@gmail.com (R.G.)

[2] Department of Chemistry, National Institute of Technology Kurukshetra, Kurukshetra 136119, India

\* Correspondence: chetti@nitkkr.ac.in (P.C.); somesh.pola@osmania.ac.in (S.P.)

**Abstract:** Under solvothermal conditions, the Zn(II) complexes formed from salophen-based ligands with N and O donor atoms are reported. These Zn(II) complexes were initially confirmed through elemental analysis and supported by mass spectral data. The purity of the ligands and Zn(II) complexes was confirmed by using NMR spectral studies. The functional group complexation was established by FT-IR analysis. Additional supportive information about the complexes is also reported through molar conductance and thermal studies. The bandgap energies of the ligands and Zn(II) complexes are estimated with UV-visible DRS studies. The rate of recombination of hole–electron pairs is directly related to photocatalytic activity, which is confirmed by using emission spectral analysis. The surface metaphors for ligands and complexes are obtained from FESEM analysis. These new sequences of Zn(II) complexes were used for the photooxidation of 2,2′-(ethyne-1,2-diyl)dianiline and its derivatives. Mechanistic studies on the fast degradation of dyes were supported in the presence of several scavengers. The rapid photooxidation process in the presence of [Zn(CPAMN)] has been demonstrated, and a highly efficient photocatalyst for the photooxidation of 2,2′-(ethyne-1,2-diyl) dianiline has been proposed. Furthermore, the experimental findings are supported by the DFT studies.

**Keywords:** Zn(II) complexes; DFT calculations; photocatalytic oxidation; rate of recombination; surface area; 2-(2-nitrophenyl)-3H-indol-3-one

## 1. Introduction

The coordination chemistry of transition metal complexes has been the subject of broad study in the past few decades. Moreover, metal–Schiff base complexes have continued to enjoy extensive magnitude owing to their structural diversity and potential applications in pharmacology and catalysis. Most of the studies have aimed to understand the role of M(II) cations in many metalloenzymes in terms of structure–function relationships [1]. The importance of transition metals in several biological systems [2] has motivated the study of the complexes of Zn(II) ions. Studies on lower/higher oxidation state complexes are of special importance because of their potential uses as oxidizing agents, catalysts [3–5] and electro-catalysts [6,7] for the oxidation of compounds such as alcohols, esters and water [8,9]. M (II) complexes with various Schiff base ligands play an important role in coordination chemistry, and a recognized Schiff base ligand is a salophen kind [10], with a bi-functional and tetradentate (-ONNO-) ligand. Some asymmetric salophen kinds of Schiff's base were described by R. Atkins [11] in 1985, who suggested a wide-ranging term for salophen kinds of tetradentate (-ONNO-) ligands. Because of the aromatic ring's substitution and outline hydroxyl group, salicylaldehyde and its analogues are suitable as building blocks for salophen-based ligands. As soon as the azomethine group is formed between the aldehyde and the primary amine, the alignment of the salophen kind of

Schiff's base [12,13] will form a new six-membered ring when it is complexed with different metal ions.

Schiff's base metal complexes with different d-block metals such as manganese [14], cobalt [15], copper [16], and zinc [17] are extensively used as catalysts in oxidation reactions. These metal complexes are active and selective catalysts in a diversity of organic transformations as well as being straightforwardly synthesized, inexpensive and stable [14]. Schiff's base ligands are typically 2-hydroxybenzaldehyde or salophen ligands. The high electron-donating capability of the Schiff bases is good for promoting the rate of electron transfer. As a result, these salophen-type ligands are being considered as potential candidates for increasing the overall catalytic performance of azomethine-functionalized complexes [18,19].

Jacobsen's catalyst is used in the well-known epoxidation reaction with a Schiff base catalyst [13,20]. At the same time, Japanese chemist, Katsuki et al., reported a very strong asymmetric epoxidation with a chiral catalyst that is correspondingly a salophen-based Mn(III) complex [21]. Several substituents at the 3,3′ and 5,5′ positions of Schiff base and an azomethine scaffold based on Jacobsen's catalyst were examined [22,23]. In the primary surveys of the (salophen) Mn(III)-catalyzed epoxidation, Zhang noticed that steric moieties such as phenyl and *t*-butyl groups at the 3,3′ location of the salophen system are crucial in the direction of attaining great enantioselectivity [13]. Metal–salophen-kind Schiff bases of uranyl complexes also play an important role as catalysts in Diels–Alder reactions [24]. Katsuki et al. reported the synthesis of asymmetric epoxidation of unfunctionalized olefins in the presence of chiral (salophen) manganese (III) complexes [23].

Zn(II) complexes include zinc carbonate, zinc acetate, zinc chloride, zinc nitrate, and zinc sulfate, along with zinc oxide, which may be of the greatest importance in affording its viable consequences as a semiconductor material [25]. Zn(II) Schiff base complexes [26] and Zn(II)-based frameworks [27] exhibit excellent photocatalytic activity.

Presently, one of the focused areas of research has been dedicated in recent years to the mixed ligand complexes of transition metals containing nitrogen and oxygen donors [28], with potential applications such as the luminescent and fluorescent detection of nitroaromatics [29,30]. In this current article, we designed and synthesized three Schiff base salophen ligands and their Zn(II) complexes and reported their photocatalytic and photooxidation studies. The significance of the present work is that all the photooxidation reactions were carried out in the presence of the Zn(II) complex and water as a solvent in visible light irradiation conditions. Moreover, the multiple photooxidation and cyclization reactions of new indol-3-one based compounds and also the amine group converted into a nitro group. Therefore, this photocatalytic reaction is a multiple photooxidation reaction.

## 2. Materials and Methods

^{1}H and ^{13}C-NMR spectra were recorded on a Bruker AV400 MHz Spectrometer with chemical shifts referenced using the ^{1}H resonance of residual CDCl$_3$ and $d_6$-DMSO. Mass spectra of the complexes were recorded by an HR-EI instrument (JEOL, Tokyo, Japan). The melting points of the complexes were verified by using a Cintex apparatus with range 50–450 °C. Thermograms of all the samples were obtained using a Shimadzu differential thermal analyzer (DTG-60H) with a heating rate of 10 °C min$^{-1}$ in the range from 50 to 1000 °C under a nitrogen-purging rate of 20 mL/minute. The surface morphology and cross-section images of the devices were taken by field-emission scanning electron microscopy (FE-SEM, ULTRA PLUS, a member of Carl Zeiss). FT-IR spectra were confirmed using Bruker spectrometer with 4 cm$^{-1}$ resolution. The phases of the new materials were established by powder X-ray diffractometer (Miniflex, Rigaku, Tokyo, Japan) (Cu K$\alpha$, $\lambda$ = 1.5406 Å angle range of 2θ = 10° to 45°). The electronic spectra were measured in CHCl$_3$/DMF (2:1) solutions on Shimadzu UV-3600 Plus UV-Vis Spectrophotometer. The photoluminescence (PL) spectra of the catalysts were documented on a Fluorescence Spectrophotometer F-7100 and with respect to their absorption maxima. All the photoreactions

were performed by using a multi-tube photo reactor system with LED visible light, Lelesil Innovative Systems, India.

## 2.1. Synthesis of $N_2$, $O_2$—Donor-Based Schiff's Base Ligands

To a solution of 2-hydroxy-1-naphthaldehyde (50 mmol) in ethanol (50 mL) at 60 °C, we added 4-chlorobenzene-1,2-diamine/4-fluorobenzene-1,2-diamine/4-methoxybenzene-1,2-diamine (25 mmol) drop wise. The resulting reaction mixture was allowed to reflux for 4 h. After the reaction mass cooled down and the solvent was taken out, a standard aqueous workup was done to obtain the ligand (Scheme 1) as 1,1′-((1E,1′E)- ((4-chloro-1,2-phenylene)bis(azanylylidene))-bis(methanylylidene))bis(naphthalen-2-ol) (CPAMN), 1,1′-((1E,1′E)-((4-fluoro-1,2-phenylene)bis(azanylylidene))-bis(methanylylidene))bis(naphthalen-2-ol) (FPAMN) and 1,1′-((1E,1′E)-((4-methoxy-1,2-phenylene)bis(azanylylidene))bis (methanylylidene))bis-(naphthalen-2-ol) (MPAMN).
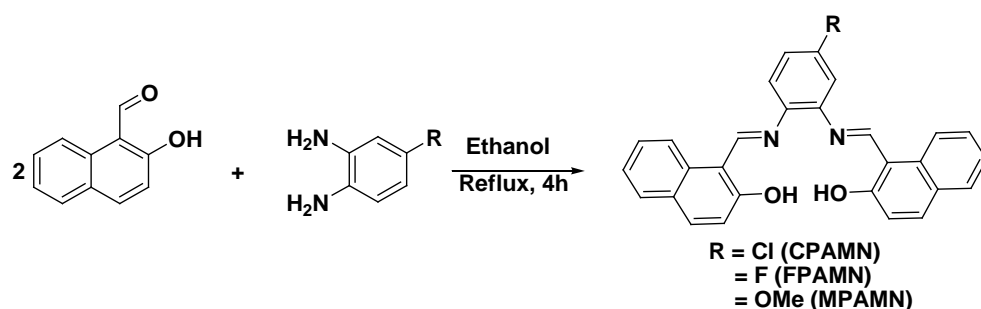


**Scheme 1.** Synthesis of new salophen-based Schiff's base ligands.

## 2.2. Synthesis of Zn(II) Complexes

The Schiff's base ligand (CPAMN/FPAMN/MPAMN) (1.00 mmol) and Zn(OAc)$_2$ (1.00 mmol) were dissolved in methanol (30 mL); then, they were heated at 60 °C under solvothermal conditions for 8 h. The solvent was evaporated under reduced pressure and recrystallized to yield microcrystalline materials with a yield of the materials 64–75% (Scheme 2).
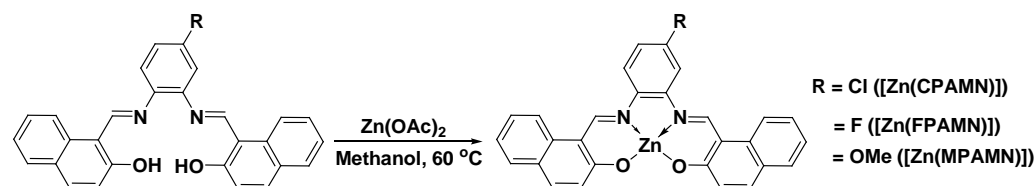


**Scheme 2.** Synthesis pathway for new Zn(II) complexes.

All the metal complexes were characterized using data from different instrumental techniques such as elemental analyses, mass spectra, $^1$H-NMR, $^{13}$C-NMR, IR studies, thermal studies, electronic spectra, and conductivity studies. The particle size and shape of complexes were examined through morphological studies by using FESEM.

## 3. Results and Discussion

The physicochemical and elemental data of both ligands (CPAMN, FPAMN and MPAMN) and Zn(II) complexes are given in Table S1. The experimental data of elements such as H, C, N, Cl, and Zn coincide with the calculated values and are equal to [Zn(CPAMN)], [Zn(FPAMN)], and [Zn(MPAMN)], respectively. The Maldi mass spectral data of the ligands and Zn(II) complexes were well-matched with the respective molecular weights of the molecules. The mass spectra of all ligands and its Zn(II) complexes (Figures S1–S6) were measured with the Maldi mass procedure (HRMS) and revealed that the base peak was given as [ML]$^+$. The *m/z* values of 513.154, 497.075, and 508.843 for Zn(II) complexes correspond to molecular ions of [Zn(CPAMN)], [Zn(FPAMN)], and

[Zn(MPAMN)], respectively [31]. These formulae are supported well by the data acquired from mass spectral studies of all the ligands and complexes.

The purity of the ligands was checked by ^{1}H-NMR spectra recorded in $d_6$-DMSO. The broad signals at δ 15.109 and 14.978 ppm are indicative of the presence of the protons of phenolic –OH groups of CPAMN ligand [32]. The singlet observed at δ 9.680 and 9.671 ppm can be assigned to the azomethine protons of the CPAMN ligand. The signals in the range of δ 8.584–7.020 ppm (Figure S7) may be attributed to the aromatic protons. Similarly, the ^{1}H-NMR spectra of the FPAMN ligand also reveal phenolic –OH groups, azomethine, and aromatic protons at 15.109, 14.979, 9.692, 9.683, and 8.593–7.029 ppm, respectively (Figure S8) [28]. In the case of the MPAMN ligand, at 15.749 ppm, phenolic protons were observed (Figure S9). As shown in Figures S7–S9, the remaining azomethine and aromatic protons are arranged in nearly the same pattern in the CPAMN, FPAMN, and MPAMN ligands. Similarly, the diamagnetic nature of Zn(II) complexes was verified by using ^{1}H-NMR spectra in $d_6$-DMSO at ambient condition (Figure S10). The disappearance of an Ar–O$\underline{H}$ protons resonance signal was observed as compared to ligands, which indicates that the ligand is complexed with $Zn^{2+}$ ions through phenolic hydroxy groups. The azomethine protons of all the three Zn complexes shifted to the deshielding by 0.12–0.20 ppm, and this indicates that the $Zn^{2+}$ ions complex with nitrogen atoms [32,33]. The remaining resonance signals of aromatic protons are moved very minor to upfield side in the ^{1}H-NMR spectrum of each complex as related to those in the spectrum of each ligand.

The imine carbon resonance signal, shown at 169.827 ppm in the spectral data of the ligand FPAMN, is found to have altered to the downfield side by 3.931 ppm. Therefore, it indicates that imine carbons were shifted toward the lower frequency side and exposes that the $Zn^{2+}$ ions complexed with nitrogen atoms [34]. All the remaining resonance signals of carbon atoms present in aromatic rings have shown a very minor shift to the deshielding in the ^{13}C-NMR spectrum of every complex as related to its ligand spectrum. The spectrum of the Zn(II) complex has shown a new signal at 188.668 ppm, which is characteristic of the coordinated phenolic carbon atom (Figure S11).

The bonding vibrational modes of all the ligands and Zn(II) complexes were recorded, and the comparison between IR spectra of ligands (CPAMN, FPAMN, and MPAMN) and their Zn(II) complexes is shown in Figure S12. The strong peaks noticed at 1645–1660 $cm^{-1}$ and 3295–3345 $cm^{-1}$ in the spectrum of ligands are recognized as the stretching vibrational modes of the imine (-C=N-) and phenolic (-OH) groups, respectively [35]. In all of the complexes, the phenolic group goes away compared to the ligand spectrum, and the imine peaks move to lower frequencies. This shows that the azomethine group is coordinated with zinc. Two new absorptions were observed in the IR spectra of the complexes when compared to their corresponding ligands; one is around 428, 436, and 419 $cm^{-1}$ (ν (Zn-N)) and the other is around 516, 522, and 518 $cm^{-1}$ (ν (Zn-O)) for [Zn(CPAMN)], [Zn(FPAMN)], and [Zn(MPAMN)], respectively. These absorptions in the IR spectra of complexes indicate that the Zn(II) ion is coordinated to the CPAMN/FPAMN/MPAMN through two imine and two phenolic -OH groups [35]. The IR spectral data of Zn(II) complexes along with details are presented in Table 1, and representative spectra are shown in Figure S12a–c.

**Table 1.** Infrared and electronic spectral data ($cm^{-1}$) of Zn(II) complexes.

| Complex | ν (Ar-OH) | ν (-C=N-) | ν (Zn-O) | ν (Zn-N) | $\lambda_{onset}$ (nm) | $E_g$ (eV) | $E_g$ (eV) (Solid State) | Surface Area ($m^2$/g) |
|---|---|---|---|---|---|---|---|---|
| CPAMN) | 3295 | 1645 | - | - | 503.66 | 2.46 | 2.75 | 65 |
| FPAMN | 3306 | 1652 | - | - | 512.39 | 2.42 | 2.72 | 59 |
| MPAMN | 3345 | 1660 | - | - | 514.52 | 2.41 | 2.87 | 57 |
| [Zn(CPAMN)] | - | 1628 | 516 | 428 | 596.15 | 2.08 | 2.18 | 208 |
| [Zn(FPAMN)] | - | 1634 | 522 | 436 | 553.57 | 2.24 | 2.15 | 184 |
| [Zn(MPAMN)] | - | 1642 | 518 | 419 | 568.80 | 2.18 | 2.24 | 169 |

The P-XRD peaks of the ligands CPAMN, FPAMN, and MPAMN exhibited 2θ values in between 5 and 3 with high-intensity peaks at 25.82°, 25.91°, and 24.79°, respectively. However, the [Zn(CPAMN), [Zn(FPAMN)], and [Zn(MPAMN)] complex peaks changed when they were linked to their respective ligands. The peaks revealed in the [Zn(CPAMN), [Zn(FPAMN), and [Zn(MPAMN)] complexes at 2θ = 9.26°, 9.28°, and 5.78° were new and intense after complexation with Zn(II) ions, whereas the peaks at 2θ = 25.82°, 25.91°, and 24.79° had a small shift and decreased in intensity (Figure 1). This indicates that Zn(II) complexes are formed with salophen ligands [36].
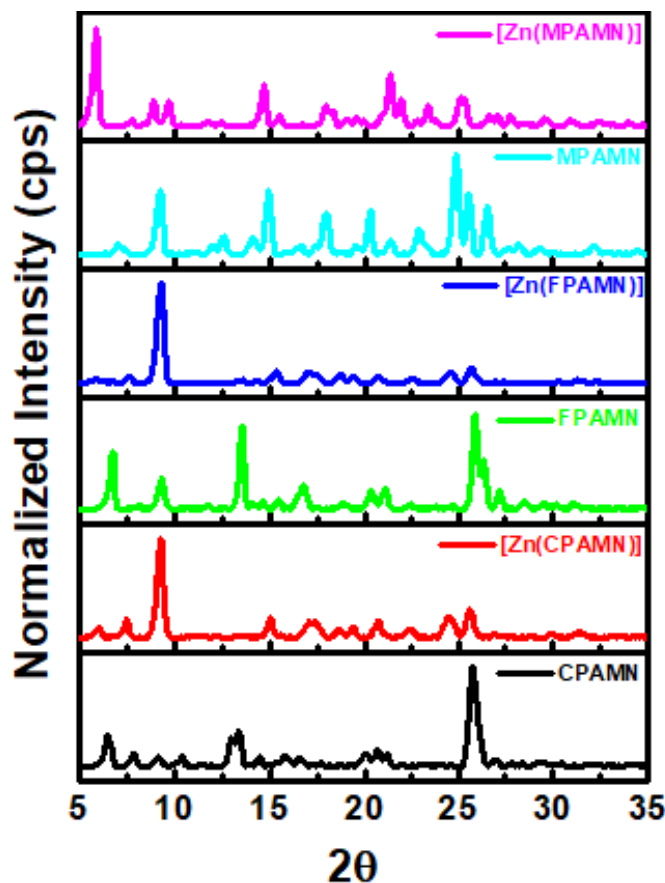


**Figure 1.** Powder XRD pattern of ligands and Zn(II) complexes.

In order to investigate the morphology features of samples, SEM characterization was performed. The results showed that there were sufficient Zn(II) complex nanofibers with a large aspect ratio, uniform diameter, and smooth surface. This was a foregone conclusion during the solvothermal synthesis of Zn(II) complex nanofibers [36]. Figure 2 shows the morphology of the molecules stirred in the ethanol solution. The results show that Zn(II) ions were able to be complexed with ligands, and the morphology of the ligands changed completely. Based on the data obtained from physicochemical and spectral studies of Zn(II) complexes, the tentative structures are shown in Scheme 2. The surface areas of the ligands CPAMN, FPAMN, and MPAMN were lower than those of Zn(II) complexes ([Zn(CPAMN], [Zn(FPAMN)], and [Zn(MPAMN)]). However, the ligand surface area is much smaller than all the complexes and is given in Table 1.
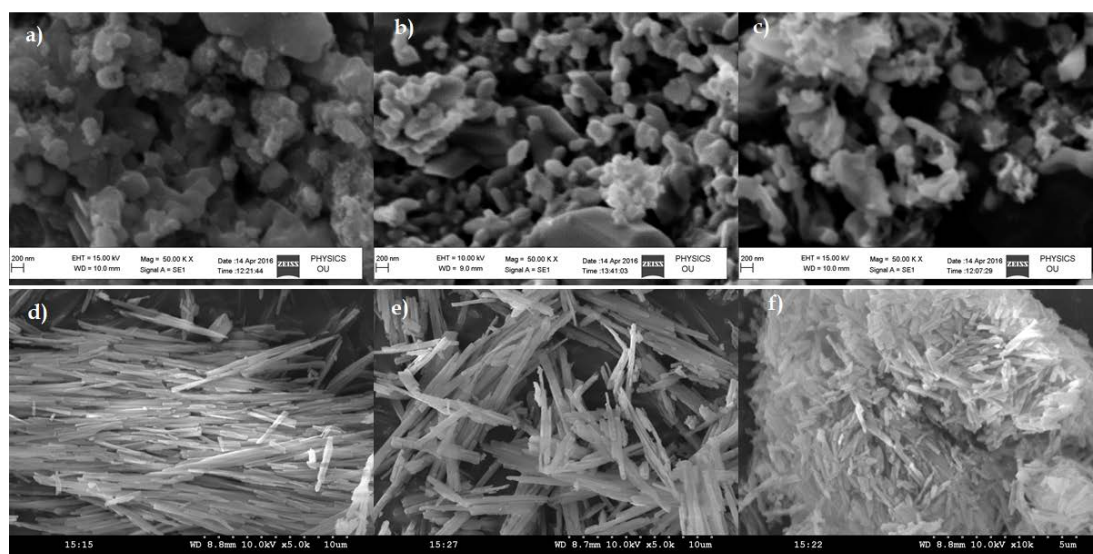
**Figure 2.** FESEM metaphors of (**a**) CPMAN, (**b**) FPMAN, (**c**) MPMAN ligands; (**d**) [Zn(CPMAN)], (**e**) [Zn(FPMAN)] and (**f**) [Zn(MPMAN)] complexes.

*3.1. Molar Conductance and Thermal Analysis*

The molar conductance of Zn(II) complexes was studied to establish the nature of the complexes, whether they are ionic or covalent in nature. The concentration of all the complexes was precise in dimethylformamide at $10^{-3}$ M. The outcomes are shown in Table S1, and the range of the molar conductance of all the complexes is 12.49 to 16.19 ohm$^{-1}$ cm$^2$ mol$^{-1}$. These data suggest that all the Zn(II) complexes were non-electrolytic in nature [37]. After 48 h of retest, the molar conductance values of each complex coincide with the initial data. Therefore, all the complexes are stable due to strong complexation with Zn(II) ions with salophen ligands.

The thermal stability of all the Zn(II) complexes was studied to understand the decomposition characteristics. The thermogravimetric data of all the Zn(II) complexes were recorded under an inert condition (N2 atmosphere) up to 800 °C with a heating rate of 10 °C min$^{-1}$ and are presented in Table S2. All the Zn(II) complexes of CPAMN, FPAMN, and MPAMN, undergo decomposition in a single stage, which indicates that the metal-to-ligand ratio is 1:1, as shown in Figure 3. The observed TG curves show that Zn(II) complexes lose their ligand part [38] at single-step weight losses of up to 84.12% (calculated 83.58%) between 250 and 700 °C. The TG curve shows a plateau from 250 to 700 °C and then no further decomposition up to 800 °C. The obtained values match with the theoretical values for the ligand part of each complex and the final part or residual mass specified as anhydrous ZnO as the final product. Therefore, the crucible consists of a small amount of undecomposed part of the complex left, which corresponds to ZnO [38].
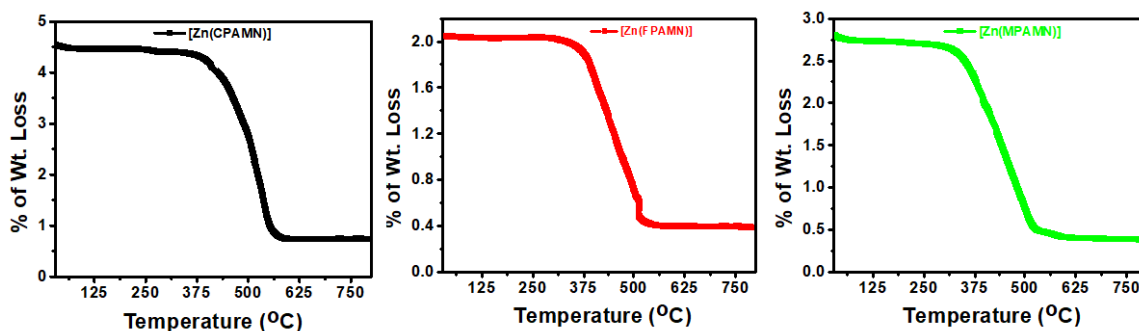


**Figure 3.** Thermograms of Zn(II) complexes.

### 3.2. Absorption and Emission Studies

The electronic spectra of Zn(II) complexes were recorded in DMF, and we also examined the solid-state UV-vis-DRS spectra, which are shown in Figure 4 and Figure S13. Each ligand consists of the three important transitions, such as $\pi \rightarrow \pi^*$ with two different aromatic rings, and another transition is $n \rightarrow \pi^*$ of the azomethine group. All of the bands in the ligand are shifted to a higher wavelength region after complexation with Zn(II) ions due to ligand to metal charge distribution via $T_{2g} \rightarrow T_{1u}$ [39]. The solution spectra of ligands CPAMN displays the bands at 318, 379, and 453 nm, respectively, whereas in the complexes [Zn(CPAMN)], they show at 331, 416, and 468 nm, respectively. Similarly, other ligands FPAMN, MPAMN, and their metal complexes also showed three bands.
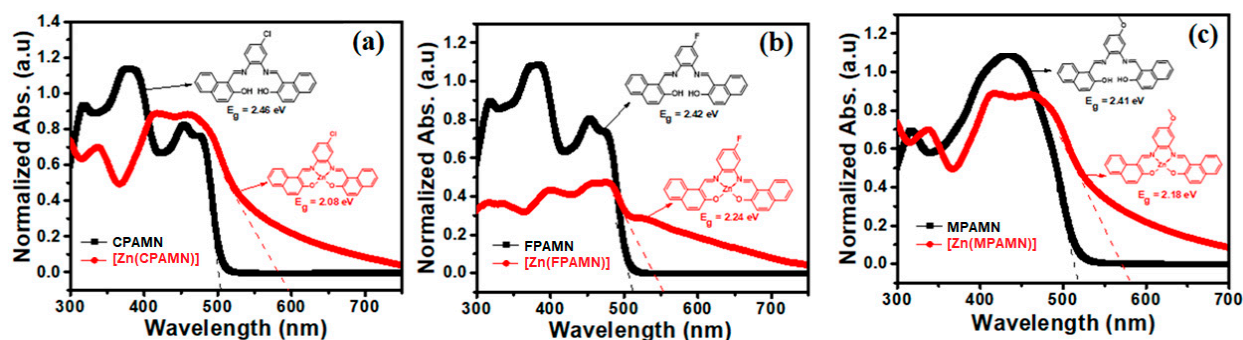


**Figure 4.** UV-visible spectra of (**a**) CPAMN and [Zn(CPAMN)], (**b**) FPAMN and [Zn(FPAMN)] and (**c**) MPAMN and [Zn(MPAMN)].

Figure S13 depicts the UV-visible diffuse reflectance spectra (UV-vis-DRS) of Zn(II) complexes, revealing that the absorption edge of the Zn(II) complexes is located in the visible light region [39]. It indicated that visible light should be selected as the driving force for the photocatalysis of these complexes. The bandgap ($E_g$) of the Zn(II) catalyst was used further for the improvement of optical performance. It can be calculated according to the following equation:

$$(\alpha h\nu) = A(E_g - h\nu)^2$$

where A is a constant, h is Planck's constant and $\nu$ is the frequency of the incident light [40]. The $E_g$ of the complexes [Zn(CPAMN)], [Zn(FPAMN)], and [Zn(MPAMN)] was 2.18, 2.15, and 2.24 eV, respectively, which was much smaller than that of standard ZnO (3.9 eV), indicating that the energy band structure of the complexes has been modified. Compared to the pure ligands CPAMN, FPAMN, and MPAMN, which were 2.75, 2.72, and 2.87 eV, respectively (Table 1), the reduced bandgap of the Zn(II) complexes made it easier to generate separated electrons and holes under the visible light radiation. Based on the above analysis, it can be concluded that the Zn(II) complexes could effectively utilize visible light to induce photocatalysis.

To get further insight into the observed electronic excitations, time-dependent density functional theory (TD-DFT) calculations have been performed for all the molecules under study [41]. The absorption properties of all the ligands have been calculated using the TD-B3LYP functional with a 6-31G(d,p) basis set. Absorption energies, oscillator strength, major transition, and percentage weight of ligand molecules are given in Table S3. The calculated absorption maximum for CPAMN, FPAMN, and MPAMN are at 437 nm, 442 nm, and 455 nm, respectively, and these are in good agreement with the experimentally observed absorption energies. All the ligands show a major transition from HOMO to LUMO.

The absorption properties of all the metal complexes have also been calculated using TD-B3LYP functional with a mixed basis set. The standard basis set of atomic functions 6-31G(d,p) was used for H, C, N, F, Cl and O atoms of metal complexes, and the LANL2DZ effective core potential basis set was used for zinc metal. The absorption values of three

complexes are shown at 453 to 459 nm (shown in Table S3). The major transitions in all the metal complexes are also from HOMO to LUMO.

Frontier molecular orbital pictures of the molecules are shown in Table S4 for ligands and metal complexes, respectively. For all ligands, the distribution of electron density in HOMO is centered on chloro, fluoro, and methoxy substituted benzene. As for the LUMO of all the molecules, electron density is spread over the acceptor (naphthalene rings) through the π-spacer (bridge), as shown in Table S4. In the case of metal complexes, the electron density in HOMO and LUMO is spread over the backbone of the ligands (Table S4). The HOMO–LUMO energy gap (HLG), along with HOMO and LUMO energies, is calculated for all the ligand molecules and is given in Table S5. The HOMO energies of CPAMN and FPAMN are −5.25 eV and −5.16 eV, respectively, which indicate the destabilization of the HOMO level on replacing Cl with an F atom. Similarly, the LUMO energies of CPAMN and FPAMN are at −1.87 eV and −1.81 eV, respectively. This result reveals that in both cases, the energy gap is nearly the same, but as we replace the Cl atom and F atom with the -OMe group at the central benzene ring, there is an increase in HOMO as well as in LUMO energy levels (destabilization), as shown in Figure 5a. The destabilization of the HOMO level is higher than the destabilization of the LUMO level, as corresponds to chloro and fluoro-substituted molecules. The calculated HOMO, LUMO energies, and the HOMO–LUMO energy gap (HLG) for metal complexes is shown in Figure 5b. The HOMO and LUMO energy levels are destabilized by Cl → F→ OMe substitution on the benzene ring, and the resultant HLG for all the three metal complexes is almost the same. It has also been calculated and found that there is not much difference in the energy gap of the three metal complexes shown in Figure 5b.
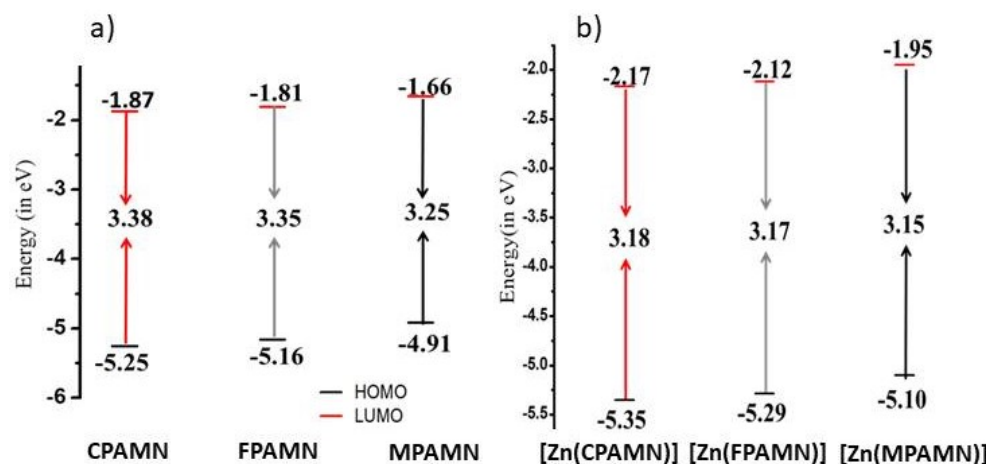


**Figure 5.** HOMO–LUMO energies and HOMO–LUMO gap of (**a**) ligands and (**b**) metal complexes.

The emission spectra of ligands and its Zn-complexes were recorded in solution. The compounds were excited at λ maxima of 480, 475, and 492 nm of ligands, whereas for Zn(II) complexes, they were at 505, 492, and 520 nm, respectively. The emission spectrum provides significant evidence about the rate of recombination of hole and electron pairs [41]. Based on this evidence, it is concluded that the ability to allocate carriers or trick charge to investigate the possible formation of electron–hole pairs from Zn(II) complexes [41]. As shown in Figure 6, the emission strength of the [Zn(CPAMN)] complex decreased completely when correlated with the [Zn(FPAMN)] and [Zn(MPAMN)]. The [Zn(CPAMN)] complex's lower emission strength indicates a low rate of recombination, implying that [Zn(CPAMN)] can benefit from hastening the separation of holes and electrons, resulting in a high photooxidation process.
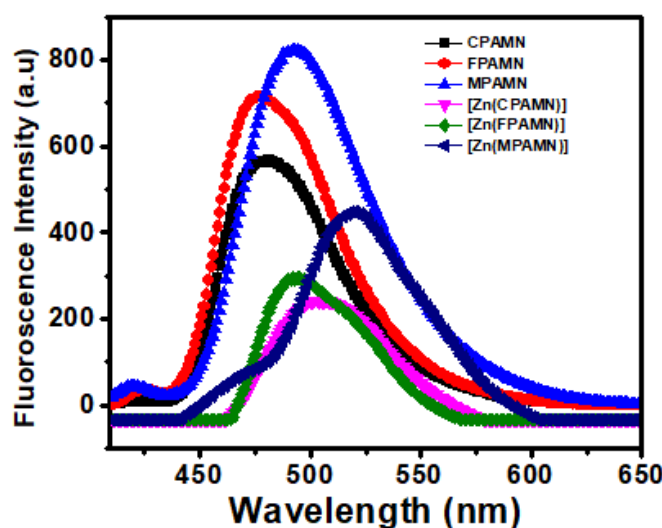
**Figure 6.** PL spectral pattern of ligands and Zn(II) complexes.

*3.3. Photocatalysis*

Under visible light source conditions, new 2-(2-nitrophenyl)-3H-indol-3-one compounds (2a–j) were synthesized in the presence of new Zn(II) complexes and an oxidant (PhI(OAc)2). The performance and stability of the catalyst play a vital role in the photocatalytic activities of the complexes [41]. The one-step synthetic pathway of 2-(2-nitrophenyl)-3H-indol-3-one and its derivatives from internal alkynes [42] is shown the in supporting information as Scheme S1. It is also noticed that the formation of 2-(2-nitrophenyl)-3H-indol-3-one (2a–j) as products at 500 watts with a tungsten lamp.

3.3.1. Optimization of Catalysis (Ligands and Zn(II) Complexes

All the ligands and Zn(II) complexes are used for photooxidation and condensation in the occurrence of visible light. The conversion of 2-(2-nitrophenyl)-3H-indol-3-one was not observed in the presence of pure ligands, whereas in the presence of Zn(II) complexes, it was shown in TLC, and after 24 h, no starting material was present (Table 2).

**Table 2.** Optimization of catalysts.

| S.No. | Intensity of the Visible Light (Tungsten) | Time (h) | % Yield Compound 5a |
|-------|-------------------------------------------|----------|---------------------|
| 1 | CPAMN | 24 | – |
| 2 | FPAMN | 24 | – |
| 3 | MPAMN | 24 | – |
| 4 | [Zn(CPAMN)] | 24 | 84 |
| 5 | [Zn(FPAMN)] | 24 | 62 |
| 6 | [Zn(MPAMN)] | 24 | 40 |

3.3.2. Identifying the Active Species and Optimization of Oxidant for Photooxidation Process

The reactive species in any photocatalytic process are four types: superoxide radical ($O_2^{\bullet-}$), hydroxyl radical ($^{\bullet}OH$), hole ($h^+$), and electron ($e^-$) [43]. The photooxidation of internal alkynes was established in the presence of Zn(II) complexes and various types of oxidants, along with scavengers, are used in the visible light irradiation technique. The effect of several oxidants was tested for photooxidation reaction promotion: of all

the oxidants tested, the strongest is PhI(OAc)$_2$ as compared to other oxidants, as shown in Table 3. Out of these four scavengers, a considerable decline in the reaction rate was observed in the presence of the O$_2$$^{\bullet-}$ scavenger (benzoquinone BQ). The existence of electron scavengers (K$_2$S$_2$O$_8$, KSO) affects the rate of photooxidation (is slower) of 2,2′-(ethyne-1,2-diyl)aniline, which indicates that the electrons also reactive species for the photooxidation procedure. As a result, these findings imply that the generated O$_2$$^{\bullet-}$ and electron (e$^-$) are the primary active species in photooxidation reactions. Hence, a photocatalytic mechanism [44] was proposed for the construction of compound 2a in the presence of Zn(II) complexes and the PhI(OAc)$_2$ system (Figure 7).

**Table 3.** Optimization of oxidant and identification active species in the presence of scavengers for conversion of 2-(2-nitrophenyl)-3H-indol-3-one.

| Oxidant | Scavenger | Time (min) | Conversion Rate |
|---|---|---|---|
| Tert-butyl peroxide | t-butyl alcohol | 24 | 10 |
| Pyridine N-oxide | t-butyl alcohol | 24 | 16 |
| 4-Methylpyridine N-oxide | t-butyl alcohol | 24 | 22 |
| (Diacetoxyiodo)benzene | t-butyl alcohol | 24 | 84 |
| Bis(tert-butylcarbonyloxy) iodobenzene | t-butyl alcohol | 24 | 69 |
| [Bis(trifluoroacetoxy)iodo]benzene | t-butyl alcohol | 24 | 74 |
| Tert-butyl peroxide | Benzoquinone | 24 | 5 |
| Pyridine N-oxide | Benzoquinone | 24 | 2 |
| 4-Methylpyridine N-oxide | Benzoquinone | 24 | trace |
| (Diacetoxyiodo)benzene | Benzoquinone | 24 | 15 |
| Bis(tert-butylcarbonyloxy) iodobenzene | Benzoquinone | 24 | 8 |
| [Bis(trifluoroacetoxy)iodo]benzene | Benzoquinone | 24 | 5 |
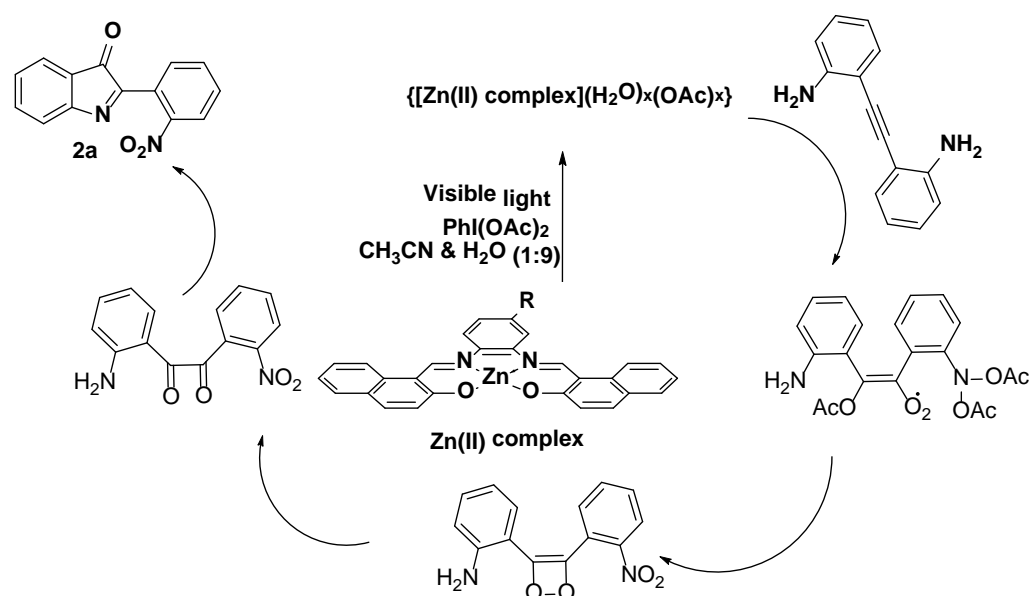


**Figure 7.** Proposal mechanism for formation of 2-(2-nitrophenyl)-3H-indol-3-one.

In this photocatalysis process, we focused mainly on three features, such as (i) variation in the strength of the energy source (effect of visible light), (ii) the effect of solvent and (iii) recyclability and stability of the catalytic system.

Effect of Visible Light Intensity

The various types of visible light sources [45] used with different intensities play a dynamic role in initializing the photooxidation and condensation in the occurrence of a photo-catalyst. The variation of the power is directly proportional to the visible light

strength, which is related to the yield and time of the final compounds as presented in Table 3. In total, 500 watts of tungsten light was used for all the reactions, and the yield of by-products (diones) was reduced by two-fold. Finally, optimization with 0.02 mmol of a photocatalyst system is sufficient to yield the 2-(2-nitrophenyl)-3H-indol-3-one (Table 4) in twenty-four hours with an obtained yield of 84%.

**Table 4.** Optimization of the intensity of visible light.



| S.No. | Intensity of the Visible Light (Tungsten) | Time (h) | % Yield Compound 5 [a] |
|---|---|---|---|
| 1 | 300 Watts | 46 | 40 |
| 2 | 400 Watts | 38 | 62 |
| 3 | 500 Watts | 24 | 84 |

[a] After purification.

Effect of Solvent

The reaction has not progressed in the absence of acetonitrile solvent (Table 5), suggesting that acetonitrile is crucial for this oxidation process. We thus studied different protic and aprotic solvents, particularly acetonitrile as an additive in $H_2O$. As shown in Table 5, the reaction was much slower in methanol, ethanol, $CH_2Cl_2$, $CHCl_3$, DMSO, toluene, and DMF than in acetonitrile.

**Table 5.** Solvent effect for the synthesis of new 2-(2-nitrophenyl)-3H-indol-3-one.

| S.No. | Solvent and $H_2O$ | Time (h) | Yield (%) Compound 2a |
|---|---|---|---|
| 1 | Toluene | 24 | 32 |
| 2 | Dichloroethane | 24 | 58 |
| 3 | THF | 24 | 35 |
| 4 | 1,4-Dioxane | 24 | 18 |
| 5 | Acetone | 24 | 21 |
| 6 | Methanol | 24 | 30 |
| 7 | Ethanol | 24 | 42 |
| 8 | $CH_3CN$ | 24 | **84** |
| 9 | DMF | 24 | 13 |
| 10 | DMSO | 24 | 9 |
| 11 | Pure $H_2O$ | 24 | **65** |

One distinguishing feature that distinguishes acetonitrile from other solvents is its oxygen solubility. Oxygen is highly soluble in acetonitrile (8.1 mM) than in other usually used organic solvents [46], such as DMSO (2.1 mM) and DMF (2.1 mM). Dioxygen plays a crucial role in this conversion. For confirmation, a controlled experiment was performed in degassed acetonitrile; only 4% yield was observed in 24 h of reaction time, as compared to 84% of compound 2a yields in acetonitrile with water (1:1). The same was performed without organic solvent; only pure water as solvent had a 65% yield. This experiment shows that $O_2$ plays a role in the oxidation of the substrates in the presence of Zn(II) complexes and the PhI(OAc)$_2$ system. It also acts as a photocatalyst, which means it helps the process go faster. Therefore, in the acetonitrile and water solvent systems, these act as proper accelerators for the consequent solvent selection.

Recyclability and Stability of the Catalytic System

Subsequently, after the completion of reactions, the suspended catalyst residue at the bottom was separated by the centrifugation process. The collected catalyst samples are of their original color, such as dark brown, indicating that the photo-oxidative product washed out the entire product present on the catalyst surface with dichloromethane to obtain the dark brown-colored catalyst [Zn(CPAMN)]. After the third rotation of the reaction, all the ^{1}H-NMR peaks are slightly broadened, as shown in Figure 8. Despite this, the [Zn(CPAMN)] photocatalyst performed 78% and slightly decreased the compound yield in the following cycle, which is due to the decreased purity of the complex [47,48]. After the photocatalysis process, the metal complexes recovered. Estimation of powder-XRD and FESEM analysis were carried out and are shown in Figures 9 and 10, respectively. As compared to the powder-XRD pattern and FESEM metaphors of pure Zn(II) complex with after photocatalysis, there was a very slight change in 2θ values, whereas there was no change in the morphology of pure and after photocatalysis.
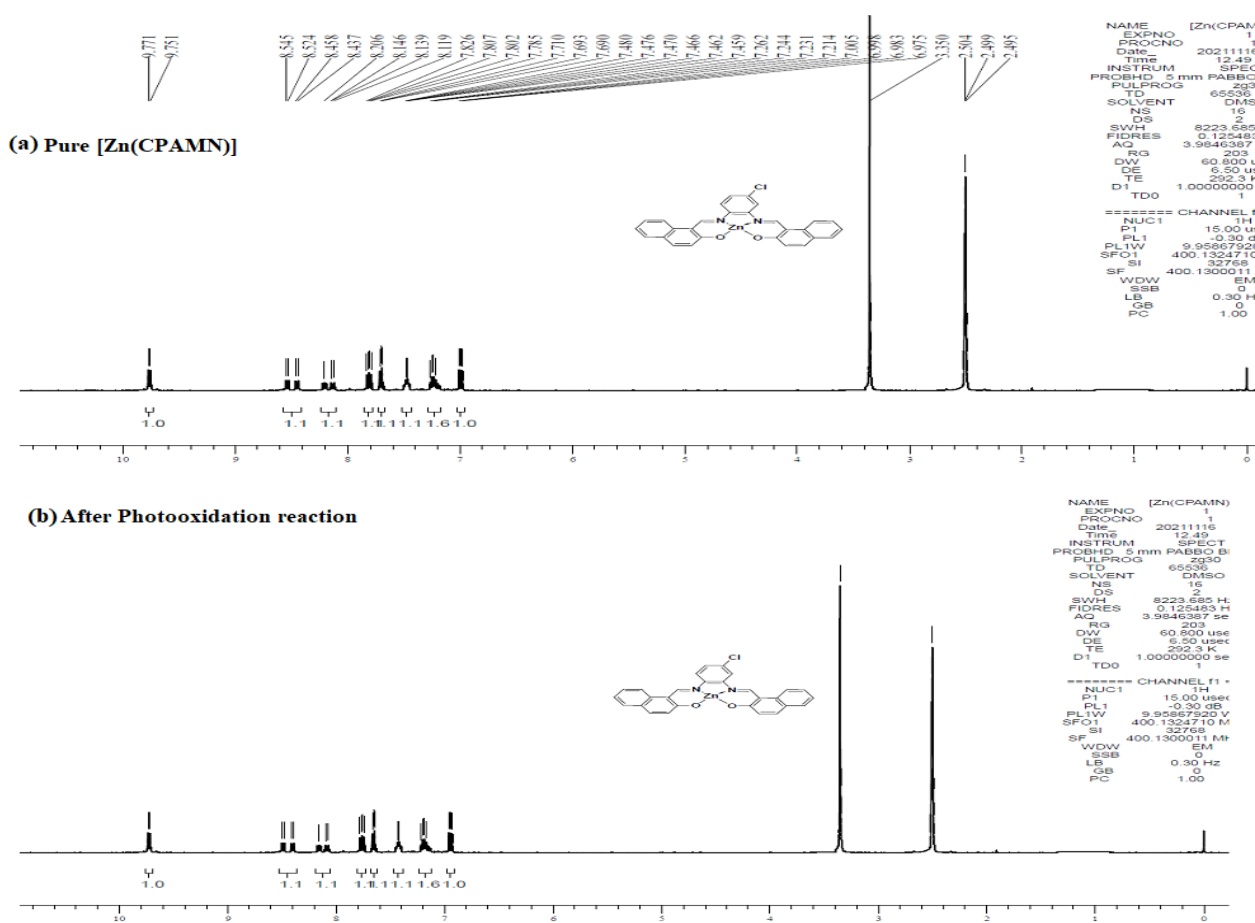


**Figure 8.** ^{1}H-NMR spectrum of (**a**) pure and (**b**) after photocatalysis [Zn(CPAMN)] complex.
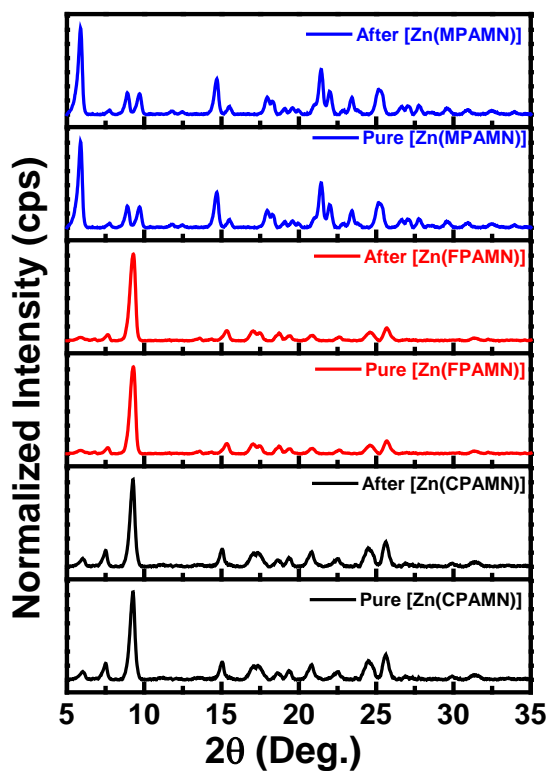
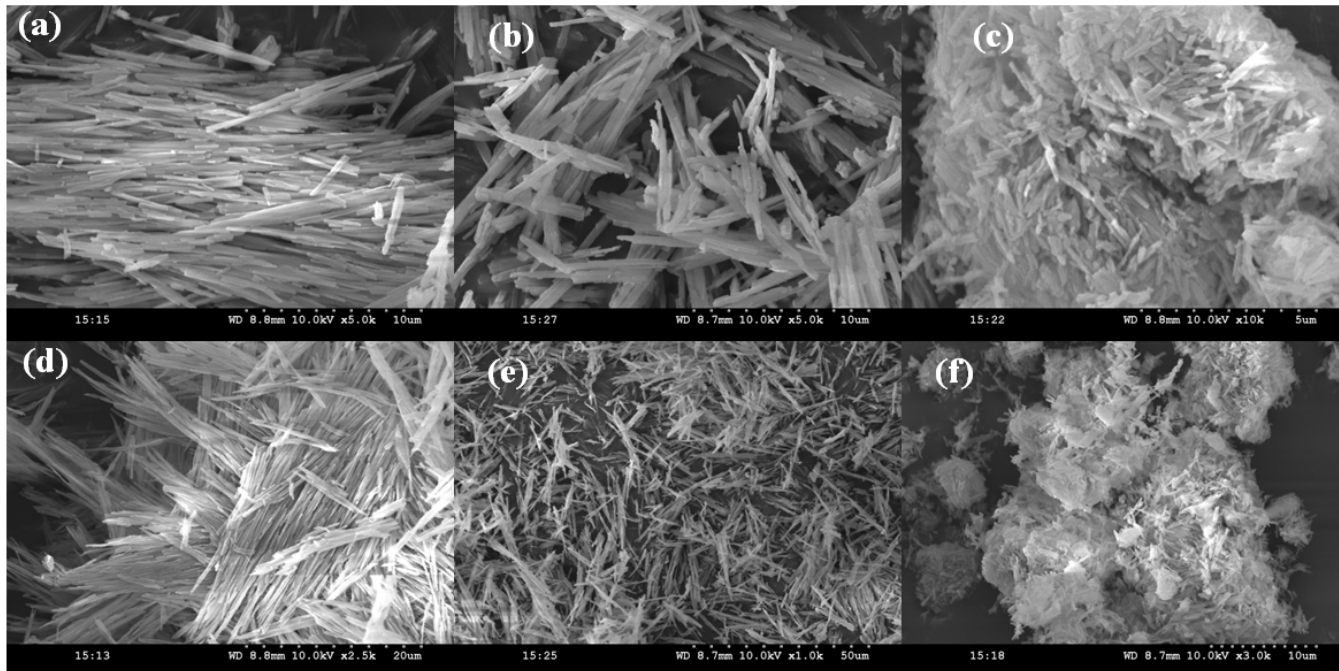**Figure 9.** Powder XRD pattern of pure and after photocatalysis Zn(II) complexes.



**Figure 10.** FESEM images of pure (**a**) [Zn(CPAMN)]; (**b**) [Zn(FPAMN)]; (**c**) [Zn(MPAMN)]; and after photocatalysis (**d**) [Zn(CPAMN)]; (**e**) [Zn(FPAMN)] and (**f**) [Zn(MPAMN)] complexes.

### 3.3.3. The Efficiency of the Photocatalyst System

As shown in Figure 11, the order of efficiency of the photocatalyst system with all substrates shows that [Zn(CPAMN)] and PhI(OAc)$_2$ are more active than both [Zn(FPAMN)] and [Zn(MPAMN)] complexes. In the Scheme S1 (supporting information), synthesis of the compound 2a is a unique pathway such as the photooxidation method, and the formation of the indolone ring containing by-product is a minor yield. All the reactants and final target molecules are shown in Table 6, and the data of the final molecules are shown in Figures S14–S33. Finally, the new [Zn(CPAMN)] complex performance was compared with some reported Zn-complexes as given in Table 7; the reported new Zn(CPAMN)] shows the better photocatalytic activity.
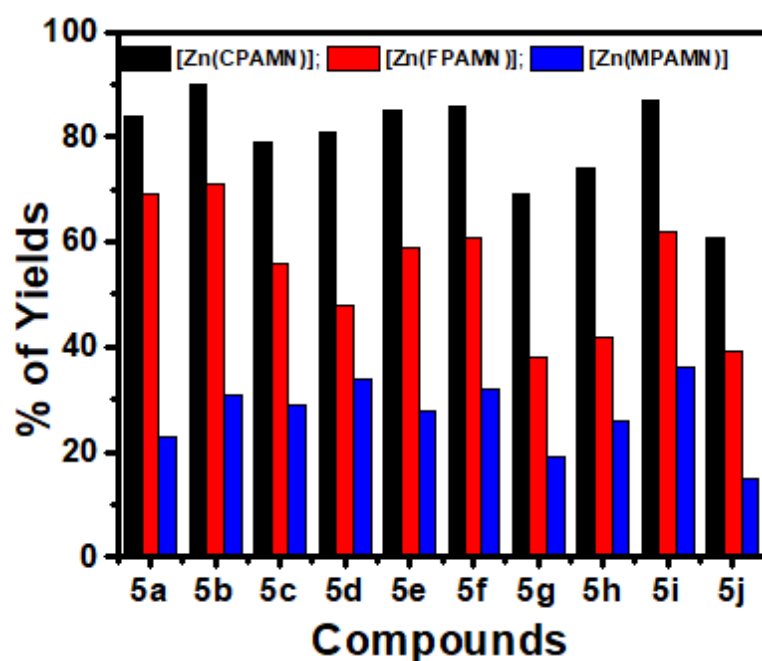


**Figure 11.** Optimization of photocatalytic performance of Zn(II) complexes.

**Table 6.** Synthesis of new 2-(2-nitrophenyl)-3H-indol-3-one and its derivatives.



| Diamine Compound | Product | Complexes | Yield % |
|---|---|---|---|
| 1a | 2a | [Zn(CPAMN)] | 84 |
| | | [Zn(FPAMN)] | 59 |
| | | [Zn(MPAMN)] | 48 |
| 1b | 2b | Zn(CPAMN)] | 90 |
| | | [Zn(FPAMN)] | 61 |
| | | [Zn(MPAMN)] | 39 |

**Table 6.** *Cont.*



| Diamine Compound | Product | Complexes | Yield % |
|---|---|---|---|
| **1c** | **2c** | Zn(CPAMN)] | 79 |
| | | [Zn(FPAMN)] | 55 |
| | | [Zn(MPAMN)] | 42 |
| **1d** | **2d** | Zn(CPAMN)] | 81 |
| | | [Zn(FPAMN)] | 49 |
| | | [Zn(MPAMN)] | 31 |
| **1e** | **2e** | Zn(CPAMN)] | 85 |
| | | [Zn(FPAMN)] | 51 |
| | | [Zn(MPAMN)] | 43 |
| **1f** | **2f** | Zn(CPAMN)] | 86 |
| | | [Zn(FPAMN)] | 49 |
| | | [Zn(MPAMN)] | 37 |
| **1g** | **2g** | Zn(CPAMN)] | 69 |
| | | [Zn(FPAMN)] | 50 |
| | | [Zn(MPAMN)] | 41 |
| **1h** | **2h** | Zn(CPAMN)] | 74 |
| | | [Zn(FPAMN)] | 38 |
| | | [Zn(MPAMN)] | 21 |
| **1i** | **2i** | Zn(CPAMN)] | 87 |
| | | [Zn(FPAMN)] | 56 |
| | | [Zn(MPAMN)] | 32 |
| **1j** | **2j** | Zn(CPAMN)] | 64 |
| | | [Zn(FPAMN)] | 35 |
| | | [Zn(MPAMN)] | 19 |

**Table 7.** Optimization of photocatalyst (PC) for conversion of 2,2′-(ethyne-1,2-diyl)dianiline into 2-(2-nitrophenyl)-3H-indol-3-one with various commercially available and new Zn(II) complexes.

| S.No. | Photocatalyst | Time (h) | Yield (%) [a] |
|---|---|---|---|
| PC-1 | Dichloro(N,N,N′,N′-tetramethylethylenediamine)zinc (28308-00-1) | 24 | – |
| PC-2 | Zinc bis[bis(trimethylsilyl)amide] (14760-26-0) | 24 | 5 |
| PC-3 | Zinc di[bis(trifluoromethylsulfonyl)imide] (168106-25-0) | 24 | 8 |
| PC-4 | Ziram (CAS No. 137-30-4) | 24 | 10 |
| PC-5 | Zinc phthalocyanine (14320-04-8) | 24 | – |
| PC-6 | [Zn(CPAMN)] | 24 | 84 |
| PC-7 | [Zn(FPAMN)] | 24 | 59 |
| PC-8 | [Zn(MPAMN)] | 24 | 48 |

[a] After purification.

## 4. Conclusions

In this study, we concluded the synthesis and account of the new three Schiff base salophen ligands and their Zn(II) complexes. The newly obtained Zn(II) complexes are examined by analytical, thermal, and spectroscopic studies. We studied the photooxidation of 2,2′-(ethyne-1,2-diyl)dianiline and its derivatives in the presence of Zn(II) complexes and converted them into new 2-(2-nitrophenyl)-3H-indol-3-one and its analogues under visible light irradiation. When compared to ligands, the bandgap energies of all Zn(II) complexes change only marginally, but their surface area increases three-fold. The outstanding photooxidation catalytic performance of [Zn(CPAMN)] is due to the low rate of recombination of hole–electron pairs, larger surface area, and low bandgap. Hence, the [Zn(CPAMN)] complex is suggested as an effective photocatalyst for the oxidation process.

# References

1. Rauscher, F.J., III.; Morris, J.F.; Tournay, O.E.; Cook, D.M.; Curran, T. Binding of the Wilms' tumor locus zinc finger protein to the EGR-1 consensus sequence. *Science* **1990**, *250*, 1259–1262. [CrossRef] [PubMed]

2. Wieghardt, K. The active sites in manganese-containing metalloproteins and inorganic model complexes. *Angew. Chem. Int. Ed. Engl.* **1989**, *28*, 1153–1172. [CrossRef]

3. Deeney, F.A.; Harding, C.J.; Morgan, G.G.; McKee, V.; Nelson, J.; Teat, S.J.; Clegg, W. Response to steric constraint in azacryptate and related complexes of iron-(II) and-(III). *J. Chem. Soc. Dalton Trans.* **1998**, *11*, 1837–1844. [CrossRef]

4. Srinivasan, K.; Michaud, P.; Kochi, J.K. Epoxidation of olefins with cationic (salophen) manganese (III) complexes. The modulation of catalytic activity by substituents. *J. Am. Chem. Soc.* **1986**, *108*, 2309–2320. [CrossRef] [PubMed]

5. Ray, M.; Mukherjee, R.; Richardson, J.F.; Buchanan, R.M. Spin-state regulation of iron (III) centres by axial ligands with tetradentate bis (picolinamide) in-plane ligands. *J. Chem. Soc. Dalton Trans.* **1993**, *16*, 2451–2457. [CrossRef]

6. Goodson, P.A.; Oki, A.R.; Glerup, J.; Hodgson, D.J. Design, synthesis, and characterization of bis (.mu.-oxo) dimanganese (III, III) complexes. Steric and electronic control of redox potentials. *J. Am. Chem. Soc.* **1990**, *112*, 6248–6254. [CrossRef]

7. Devereux, M.; McCann, M.; Leon, V.; Geraghty, M.; McKee, V.; Wikaira, J. Synthesis and fungitoxic activity of manganese (II) complexes of fumaric acid: X-ray crystal structures of [Mn(fum)(bipy)(H$_2$O)] and [Mn(Phen)$_2$(H$_2$O)$_2$](fum)·4H$_2$O (fumH$_2$=fumaric acid; bipy=2,2′-bipyridine; phen=1,10-phenanthroline). *Polyhedron* **2000**, *19*, 1205–1211. [CrossRef]

8. Gultneh, Y.; Yisgedu, T.B.; Tesema, Y.T.; Butcher, R.J. Dioxo-bridged dinuclear manganese (III) and-(IV) complexes of pyridyl donor tripod ligands: Combined effects of steric substitution and chelate ring size variations on structural, spectroscopic, and electrochemical properties. *Inorg. Chem.* **2003**, *42*, 1857–1867. [CrossRef]

9. Biswas, S.; Mitra, K.; Chattopadhyay, S.K.; Adhikary, B.; Lucas, C.R. Mononuclear manganese (II) and manganese (III) complexes of N2O donors involving amine and phenolate ligands: Absorption spectra, electrochemistry and crystal structure of [Mn (L$_3$)$_2$](ClO$_4$). *Transit. Met. Chem.* **2005**, *30*, 393–398. [CrossRef]

10. Ebrahimipour, S.Y.; Maryam, M.; Masoud, T.M.; Jim, S.; Joel, T.M.; Iran, S. Synthesis and structure elucidation of novel salophen-based dioxo-uranium (VI) complexes: In-vitro and in-silico studies of their DNA/BSA-binding properties and anticancer activity. *Eur. J. Med. Chem.* **2017**, *140*, 172–186. [CrossRef]

11. Atkins, R.; Brewer, G.; Kokot, E.; Mockler, G.M.; Sinn, E. Copper (II) and nickel (II) complexes of unsymmetrical tetradentate Schiff base ligands. *Inorg. Chem.* **1985**, *24*, 127–134. [CrossRef]

12. Kushwah, N.P.; Pal, M.K.; Wadawale, A.P.; Jain, V.K. Diorgano-gallium and-indium complexes with salophen ligands: Synthesis, characterization, crystal structure and C–C coupling reactions. *J. Organomet. Chem.* **2009**, *694*, 2375–2379. [CrossRef]

13. Zhang, W.; Loebach, J.L.; Wilson, S.R.; Jacobsen, E.N. Enantioselective epoxidation of unfunctionalized olefins catalyzed by salophen manganese complexes. *J. Am. Chem. Soc.* **1990**, *112*, 2801–2803. [CrossRef]

14. Rong, M.; Wang, J.; Shen, Y.; Han, J. Catalytic oxidation of alcohols by a novel manganese Schiff base ligand derived from salicylaldehyd and l-Phenylalanine in ionic liquids. *Catal. Commun.* **2012**, *20*, 51–53. [CrossRef]

15. Kervinen, K.; Korpi, H.; Leskelä, M.; Repo, T. Oxidation of veratryl alcohol by molecular oxygen in aqueous solution catalyzed by cobalt salophen-type complexes: The effect of reaction conditions. *J. Mol. Catal. A Chem.* **2003**, *203*, 9–19. [CrossRef]

16. Soroceanu, A.; Cazacu, M.; Shova, S.; Turta, C.; Kožíšek, J.; Gall, M.; Breza, M.; Rapta, P.; Mac Leod, T.C.; Pombeiro, A.J. Copper (II) complexes with Schiff bases containing a disiloxane unit: Synthesis, structure, bonding features and catalytic activity for aerobic oxidation of benzyl alcohol. *Eur. J. Inorg. Chem.* **2013**, *2013*, 1458–1474. [CrossRef]

17. Huang, S.; Zou, L.-Y.; Ren, A.-M.; Guo, J.-F.; Liu, X.-T.; Feng, J.-K.; Yang, B.-Z. Computational design of two-photon fluorescent probes for a zinc ion based on a salophen ligand. *Inorg. Chem.* **2013**, *52*, 5702–5713. [CrossRef]

18. Tarade, K.; Shinde, S.; Sakate, S.; Rode, C. Pyridine immobilised on magnetic silica as an efficient solid base catalyst for Knoevenagel condensation of furfural with acetyl acetone. *Catal. Commun.* **2019**, *124*, 81–85. [CrossRef]

19. Hu, J.; Li, K.; Li, W.; Ma, F.; Guo, Y. Selective oxidation of styrene to benzaldehyde catalyzed by Schiff base-modified ordered mesoporous silica materials impregnated with the transition metal-monosubstituted Keggin-type polyoxometalates. *Appl. Catal. A Gen.* **2009**, *364*, 211–220. [CrossRef]

20. Jacobsen, E.N.; Zhang, W.; Muci, A.R.; Ecker, J.R.; Deng, L. Highly enantioselective epoxidation catalysts derived from 1,2-diaminocyclohexane. *J. Am. Chem. Soc.* **1991**, *113*, 7063–7064. [CrossRef]

21. Irie, R.; Noda, K.; Ito, Y.; Matsumoto, N.; Katsuki, T. Catalytic asymmetric epoxidation of unfunctionalized olefins. *Tetrahedron Lett.* **1990**, *31*, 7345–7348. [CrossRef]

22. McGarrigle, E.M.; Gilheany, D.G. Chromium− and manganese−salophen promoted epoxidation of alkenes. *Chem. Rev.* **2005**, *105*, 1563–1602. [CrossRef] [PubMed]

23. Irie, R.; Noda, K.; Ito, Y.; Matsumoto, N.; Katsuki, T. Catalytic asymmetric epoxidation of unfunctionalized olefins using chiral (salophen) manganese (III) complexes. *Tetrahedron Asymmetry* **1991**, *2*, 481–494. [CrossRef]

24. Dalla Cort, A.; Mandolini, L.; Schiaffino, L. Exclusive transition state stabilization in the supramolecular catalysis of Diels–Alder reaction by a uranyl salophen complex. *Chem. Commun.* **2005**, *30*, 3867–3869. [CrossRef]

25. Chen, C.; Liu, P.; Lu, C. Synthesis and characterization of nano-sized ZnO powders by direct precipitation method. *Chem. Eng. J.* **2008**, *144*, 509–513. [CrossRef]

26. Patel, U.; Parmar, B.; Dadhania, A.; Suresh, E. Zn(II)/Cd(II)-Based Metal–Organic Frameworks as Bifunctional Materials for Dye Scavenging and Catalysis of Fructose/Glucose to 5-Hydroxymethylfurfural. *Inorg. Chem.* **2021**, *60*, 9181–9191. [CrossRef]

27.  Chimupala, Y.; Kaeosamut, N.; Yimklan, S. Octahedral to Tetrahedral Conversion upon a Ligand-Substitution-Induced Single-Crystal to Single-Crystal Transformation in a Rectangular Zn(II) Metal–Organic Framework and Its Photocatalysis. *Cryst. Growth Des.* **2021**, *21*, 5373–5382. [CrossRef]
28.  Bhattacharjee, C.H.; Das, G.; Mondal, P.; Rao, N.V.S. Novel photoluminescent hemi-disclike liquid crystalline Zn(II) complexes of [$N_2O_2$] donor 4-alkoxy substituted salicyldimine Schiff base with aromatic spacer. *Polyhedron* **2010**, *29*, 3089–3096. [CrossRef]
29.  Song, X.; Yu, H.; Yan, X.; Zhang, Y.; Miao, Y.; Ye, K.; Wang, Y. A luminescent benzothiadiazole-bridging bis(salicylaldiminato)zinc(II) complex with mechanochromic and organogelation properties. *Dalton Trans.* **2018**, *47*, 6146–6155. [CrossRef]
30.  Germain, M.E.; Vargo, T.R.; Khalifah, P.G.; Knapp, M.J. Fluorescent detection of nitroaromatics and 2,3-dimethyl-2,3-dinitrobutane (DMNB) by a Zinc complex: (salophen)Zn. *Inorg. Chem.* **2007**, *46*, 4422–4429. [CrossRef]
31.  Dalla Cort, A.; Mandolini, L.; Pasquini, C.; Rissanen, K.; Russo, L.; Schiaffino, L. Zinc–salophen complexes as selective receptors for tertiary amines. *New J. Chem.* **2007**, *31*, 1633–1638. [CrossRef]
32.  Swamy, S.J.; Pola, S. Spectroscopic studies on Co(II), Ni(II), Cu(II) and Zn(II) complexes with a $N_4$-macrocylic ligands. *Spectrochim. Acta Part A Mol. Biomol. Spectrosc.* **2008**, *70*, 929–933. [CrossRef] [PubMed]
33.  Tiwari, A.; Mishra, A.; Mishra, S.; Mamba, B.; Maji, B.; Bhattacharya, S. Synthesis and DNA binding studies of Ni (II), Co (II), Cu (II) and Zn(II) metal complexes of N1, N5-bis [pyridine-2-methylene]-thiocarbohydrazone Schiff-base ligand. *Spectrochim. Acta Part A Mol. Biomol. Spectrosc.* **2011**, *79*, 1050–1056. [CrossRef] [PubMed]
34.  Asadi, M.; Asadi, Z.; Torabi, S.; Lotfi, N. Synthesis, characterization and thermodynamics of complex formation of some new Schiff base ligands with some transition metal ions and the adduct formation of zinc Schiff base complexes with some organotin chlorides. *Spectrochim. Acta Part A Mol. Biomol. Spectrosc.* **2012**, *94*, 372–377. [CrossRef] [PubMed]
35.  Nawar, N.; Hosny, N.M. Synthesis, spectral and antimicrobial activity studies of o-aminoacetophenone o-hydroxybenzoylhydrazone complexes. *Transit. Met. Chem.* **2000**, *25*, 1–8. [CrossRef]
36.  Dharnipathi, V.R.; Subburu, M.; Gade, R.; Basude, M.; Chetti, P.; Simhachalam, N.B.; Nagababu, P.; Bhongiri, Y.; Pola, S. A new Zn(II) complex-composite material: Piezoenhanced photomineralization of organic pollutants and wastewater from the lubricant industry. *Environ. Sci. Water Res. Technol.* **2021**, *7*, 1737–1747.
37.  Geary, W.J. The use of conductivity measurements in organic solvents for the characterisation of coordination compounds. *Coord. Chem. Rev.* **1971**, *7*, 81–122. [CrossRef]
38.  Ahemed, J.; Pasha, J.; Kore, R.; Gade, R.; Bhongiri, Y.; Chetti, P.; Pola, S. Synthesis of new Zn(II) complexes for photo decomposition of organic dye pollutants, industrial wastewater and photo-oxidation of methyl arenes under visible-light. *J. Photochem. Photobiol. A Chem.* **2021**, *419*, 113455. [CrossRef]
39.  Manoj Kr., P.; Singh, Y.D.; Singh, N.B.; Sarkar, U. Emissive bis-salicylaldiminato schiff base ligands and their zinc(II)complexes: Synthesis, photophysical properties, mesomorphism and DFT studies. *J. Mol. Struct.* **2015**, *1081*, 316–328.
40.  Subburu, M.; Gade, R.; Guguloth, V.; Chetti, P.; Ravulapelly, K.R.; Pola, S. Effective photodegradation of organic pollutantsin the presence of mono and bi-metallic complexes under visible-light irradiation. *J. Photochem. Photobiol. A Chem.* **2021**, *406*, 112996. [CrossRef]
41.  Frisch, M.J.; Trucks, G.W.; Schlegel, H.B.; Scuseria, G.E.; Robb, M.A.; Cheeseman, J.R.; Scalmani, G.; Barone, V.; Mennucci, B.; Petersson, G.A.; et al. *Gaussian 09, Revision E.01*; Gaussian, Inc.: Wallingford, CT, USA, 2009.
42.  Yang, X.-J.; Chen, B.; Li, X.-B.; Zheng, L.-Q.; Wu, L.-Z.; Tung, C.-H. Photocatalytic organic transformation by layered double hydroxides: Highly efficient and selective oxidation of primary aromatic amines to their imines under ambient aerobic conditions. *Chem. Commun.* **2014**, *50*, 6664–6667. [CrossRef] [PubMed]
43.  Luís, M.T.F.; Amin, I.; Maria, L.S.C. Photochemical Transformations of Tetrazole Derivatives: Applications in Organic Synthesis. *Molecules* **2010**, *15*, 3757–3774.
44.  Shi, L.; Liang, L.; Ma, J.; Wang, F.; Sun, J. Enhanced photocatalytic activity over the $Ag_2O$–$gC_3N_4$ composite under visible light. *Catal. Sci. Technol.* **2014**, *4*, 758–765. [CrossRef]
45.  Zhu, X.; Li, P.; Shi, Q.; Wang, L. Thiyl radical catalyzed oxidation of diarylalkynes to α-diketones by molecular oxygen under visible-light irradiation. *Green Chem.* **2016**, *18*, 6373–6379. [CrossRef]
46.  Guguloth, V.; Ahemed, J.; Subburu, M.; Guguloth, V.C.; Chetti, P.; Pola, S. A very fast photodegradation of dyes in the presence of new Schiff's base $N_4$-macrocyclic Ag-doped Pd (II) complexes under visible-light irradiation. *J. Photochem. Photobiol. A Chem.* **2019**, *382*, 111975. [CrossRef]
47.  Li, Y.; Lee, T.B.; Wang, T.; Gamble, A.V.; Gorden, A.E. Allylic C–H Activations Using Cu(II) 2-Quinoxalinol Salophen and tert-Butyl Hydroperoxide. *J. Org. Chem.* **2012**, *77*, 4628–4633. [CrossRef]
48.  Pola, S.; Subburu, M.; Guja, R.; Muga, V.; Tao, Y.-T. New photocatalyst for allylic aliphatic C–H bond activation and degradation of organic pollutants: Schiff base Ti(IV) complexes. *RSC Adv.* **2015**, *5*, 58504–58513. [CrossRef]